Journal of Geophysical Research: Oceans

Key Points:
- We provide a time series of seawater barium measurements from the Arctic winter through summer
- We provide evidence for nonconservative behavior of barium in sea-ice
- Our findings show that the assumptions surrounding the use of barium as a freshwater tracer in the Arctic need to be challenged

Supporting Information:
- Supporting Information S1

Correspondence to:
K. Hendry,
K.Hendry@bristol.ac.uk

Spatiotemporal Variability of Barium in Arctic Sea-Ice and Seawater

Katharine R. Hendry[1], Kimberley M. Pyle[1], G. Barney Butler[1], Adam Cooper[1,2], Agneta Fransson[3], Melissa Chierici[4], Melanie J. Leng[5,6], Amelie Meyer[3], and Paul A. Dodd[3]

[1]School of Earth Sciences, University of Bristol, Wills Memorial Building, Bristol, UK, [2]Ocean and Earth Science, University of Southampton, National Oceanography Centre Southampton, Empress Dock, European Way, Southampton, UK, [3]Norwegian Polar Institute, Fram Centre, Tromsø, Norway, [4]Institute of Marine Research, Tromsø, Norway, [5]NERC Isotope Geosciences Laboratory, Keyworth, Nottingham, UK, [6]School of Biosciences, The University of Nottingham, Sutton Bonington Campus, Leicestershire, UK

Abstract Freshwater export from the Arctic is critical in determining the density of water at sites of North Atlantic deep water formation, which in turn influences the global flux of oceanic heat and nutrients. We need geochemical tracers and high-resolution observations to refine our freshwater budgets and constrain models for future change. The use of seawater barium concentrations in the Arctic Ocean as a freshwater tracer relies on the conservative behavior of barium in seawater; while this has been shown to be an unreliable assumption in Arctic summers, there are a lack of studies observing seasonal progressions. Here, we present barium concentrations from seawater and sea-ice collected during the Norwegian Young Sea ICE expedition from boreal winter into summer. We use other tracers (salinity, oxygen isotopes, and alkalinity) to reconstruct freshwater inputs and calculate a barium "deficit" that can be attributed to nonconservative processes. We locate a deficit in winter when biological production is low, which we attribute to uptake by barite formation associated with old organic matter or by internal sea-ice processes. We also find a significant barium deficit during the early spring bloom, consistent with uptake into organic-matter associated microenvironments. However, in summer, there no strong barium deficit near the surface, despite high biological production and organic carbon standing stocks, perhaps reflecting phytoplankton assemblage changes, and/or rapid internal cycling. Our findings challenge the assumptions surrounding the use of barium as an Arctic freshwater tracer, and highlight the need to improve our understanding of barium in sea-ice environments.

1. Introduction

The balance of fresh and marine waters in the Arctic is critical in determining the mixing of nutrients, high-latitude heat fluxes, and the density of seawater exported to the North Atlantic. There has been an increasing concern about changes in the characteristics of water masses in the Arctic in recent decades, in particular subsurface temperatures, and how these changes influence regional heat fluxes, biological production, and carbon export (Alexeev et al., 2013; Smedsrud, 2005). Understanding such processes and their influence on these climatically sensitive regions requires a robust quantification of freshwater inputs, and the subsequent physical, chemical, and biological responses of the Arctic system.

Total barium concentration, [Ba], has been used extensively in the Arctic Ocean—in conjunction with seawater salinity, oxygen isotope ratios ($\delta^{18}O_w$), and total alkalinity (A_T)—as a tracer of freshwater inputs (Cooper et al., 2008; Taylor et al., 2003). Salinity, $\delta^{18}O_w$, and A_T are used together to calculate the total amount of meteoric water contributing to the freshwater flux (as opposed to sea-ice melt) (Chierici et al., 2011; Fransson et al., 2001); [Ba] is then used as a further nuanced constraint to determine the input of rivers (Dodd et al., 2009; Macdonald et al., 1999; Thomas et al., 2011) or oceanic basins (Abrahamsen et al., 2009).

The use of [Ba] as a riverine input proxy relies on two key, but challengeable, assumptions: that the relationship between [Ba] and the various end-member inputs is constant, and that barium behaves conservatively within the water column once it has entered the marine system. First, the compositions of the various inputs, including Arctic rivers, glacial meltwaters, groundwaters, submarine discharge, sea-ice and snow pack, are poorly constrained. Second, rather than showing typical conservative behavior, dissolved [Ba]

generally shows a "nutrient-like" profile, exhibiting a strong relationship in seawater with dissolved silicon and alkalinity on regional and global scales (Jacquet et al., 2005; Jeandel et al., 1996; Pyle et al., 2017). Furthermore, particulate barium—largely in the form of barium sulfate or barite—shows strong links with particulate organic carbon. Specifically, particulate "excess Ba" (Ba_{xs} i.e., any Ba that is present in particles that is unsupported by lithogenic material) correlates with the flux of particulate organic carbon (POC) measured in suspended particulates (Dehairs et al., 1991; Thomas et al., 2011), sediment traps (Cardinal et al., 2005), and seafloor sediments (Eagle et al., 2003). More recent studies, including those utilizing marine barium isotopes, also highlight the nonconservative behavior of barium in near surface waters (Bates et al., 2017; Horner et al., 2015; Hsieh & Henderson, 2017; Jullion et al., 2017).

These two critical assumptions may also be questioned in the specific conditions of the Arctic, in particular as a result of biological uptake in the Arctic summer, which leads to barium drawdown associated with organic matter (Abrahamsen et al., 2009; Thomas et al., 2011). Other studies suggest that nonconservative behavior may originate in high-latitude sea-ice zones that are independent of silicon cycling and other indicators of biological activity (Pyle et al., 2017). Here, we examine these assumptions using a seasonal data set of sea-ice and underlying seawater samples collected in the region north of Svalbard, the Nansen Basin and shelf slopes, during the Norwegian young sea ICE expedition (N-ICE2015) (Granskog et al., 2016). Our analyses highlight the nonconservative behavior of barium in seawater under both true Arctic winter conditions in addition to during spring and summer algal blooms, which has important implications for the use of [Ba] as a tracer in Arctic waters.

2. Methods and Materials

2.1. Sample Collection

Seawater and sea-ice samples were collected on board the *R/V Lance* as part of the Norwegian Young Sea ICE expedition (N-ICE2015) project (January–June 2015; Figure 1a). The N-ICE drift expedition comprised four Floes from January to June 2015. Full details of the Floes are given in the supporting information. All seawater samples were collected using Niskin bottles deployed through holes in the sea-ice from the CTD rosette on the ship, or from casts taken through the sea-ice in a tent away from the ship, and stored in acid-cleaned HDPE bottles for barium. Samples for salinity were stored in sealed glass bottles until onboard-ship analysis and for A_T in borosilicate glass bottles until analysis on shore (Fransson et al., 2017). Ice cores were drilled with an ice corer (Mark II coring system, KOVACS enterprise, USA), subsectioned and allowed to melt in a sealed container in darkness overnight (Assmy et al., 2017; Fransson et al., 2015; Kauko et al., 2017) before being sampled cleanly into acid-washed HDPE bottles for barium and in borosilicate bottles for A_T (Fransson et al., 2015).

2.2. Oceanographic Setting

The hydrography of the N-ICE2015 sections used in this study (Figure 1b, see supporting information Figure S5 for T-S plot) was characterized by typical Arctic Ocean water column structure, with cold, fresh Polar Surface Water (PSW) separated by a strong halocline from underlying warm Atlantic Water (AW). The Mixed Layer Depth (MLD) during the N-ICE2015 expedition ranged from approximately 100–200 m in winter, shoaling to less than 20 m after 26 May concurrently with a shallowing of the pycnocline (Meyer et al., 2017b). The average depth of AW before 26 May was approximately 150 m and decreased to approximately 50 m after the 26 May 2015, over the Yermak Plateau (Meyer et al., 2017a). Vertical mixing in the Arctic Ocean results largely from the action of winds and internal tides (Rippeth et al., 2015). It should be noted that the N-ICE2015 "winter" and "summer" sampling does not strictly define a true seasonal time series: the winter samples are collected in a region that is likely to represent Arctic Ocean conditions; however, the summer samples are collected in a region of continual AW incursion near the slope environment where tidal forcing is stronger and the MLD is likely to be permanently shallow. A complete description of oceanographic conditions is presented in Meyer et al. (2017b). Heat fluxes from the warmer southern-sourced AW contribute significantly in this region north of Svalbard to the melting of Arctic sea ice, especially in regions of rough, shallow topography (Rippeth et al., 2015; Sirevaag & Fer, 2009; Smedsrud, 2005). During this study, the ocean-ice heat fluxes were highly variable and were driven strongly by wind forcing, internal tides, and water mass incursions (Koenig et al., 2016). Each drift started in pack ice, with distance to open water declining through time for each Floe (Meyer et al., 2017b). There was no thermodynamic ice formation during the
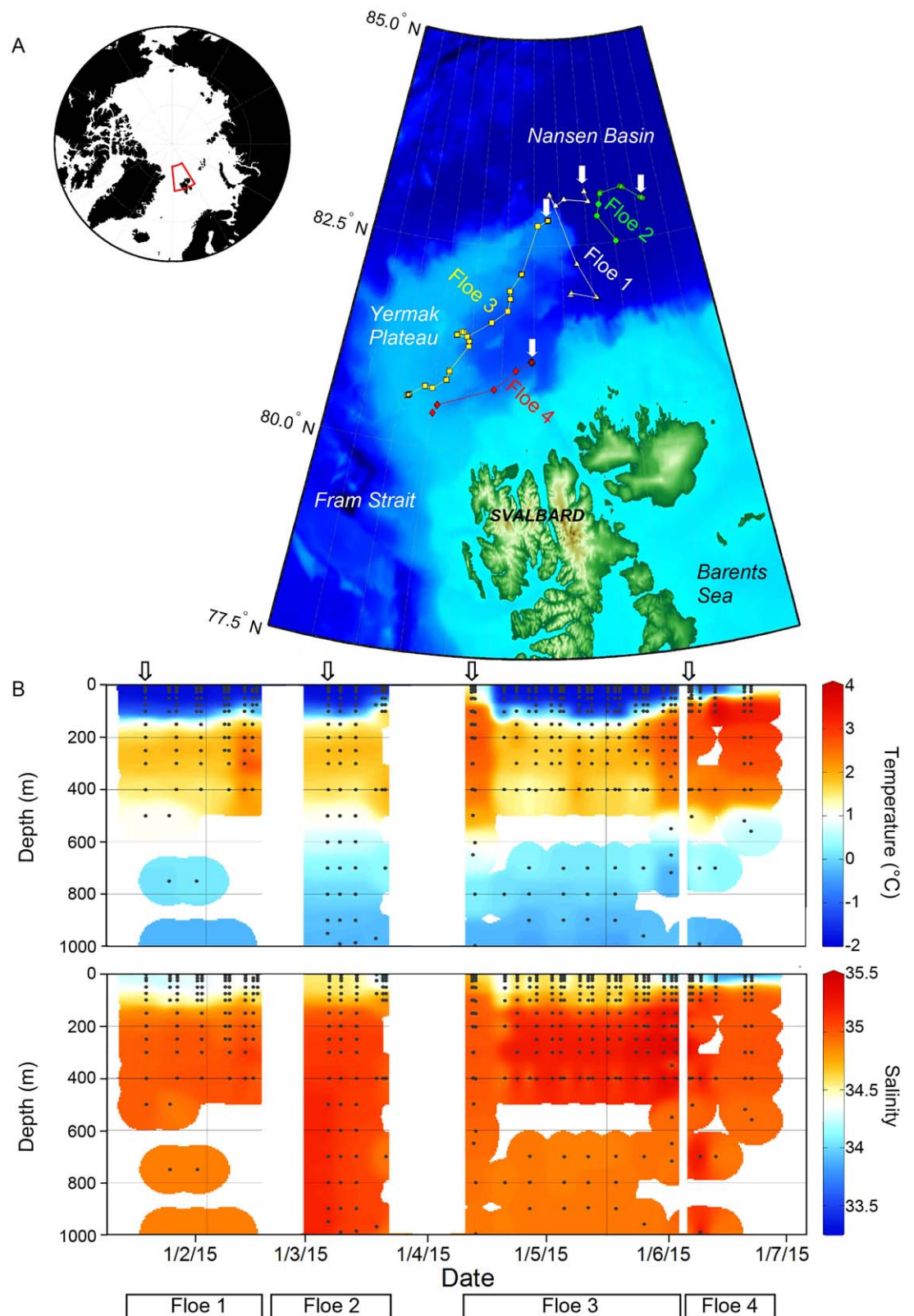
Figure 1. (a) Map of sampling locations during N-ICE2015 (red box shows expanded map area), color-coded according to Floe number (see supporting information for Floe details); (b) Hydrographic time-series for stations used in this study, with (top) temperature and (bottom) salinity. Floe numbers are marked in white boxes. Arrows mark the first CTD of each Floe used in this study.

period of study, although there were flooding and snow-ice transformations throughout the sampling period (Granskog et al., 2016; Provost et al., 2017). In January and February, there was relatively slow sea-ice drift with respect to wind speed, the sea-ice drift sped up later in the winter and into the spring concurrent with irreversible damage caused by a large storm events (Itkin et al., 2017).

During the winter months, biological activity in the water column was very low (Chlorophyll a [Chl a] below $\sim$0.1 mg/m^3). After 26 May 2015, a phytoplankton bloom dominated by *Phaeocystis* developed under the ice due to strong lead formation (Chl a 1–8 mg/m^3), POC, and decline in total dissolved inorganic carbon (DIC; Assmy et al., 2016, 2017; Fransson et al., 2017). Diatoms were not the most abundant phytoplankton, although sea-ice diatoms (e.g., *Nitzschia*) were found predominantly in first-year ice with multiyear ice forming an important winter "repository" of sea-ice algae that supplied cells to younger ice in the spring and summer (Olsen et al., 2017).

2.3. Analytical Methods

All samples were unfiltered and equilibrated over several months, such that the [Ba] measurements represent total reactive barium (Guay & Falkner, 1997). Seawater and sea-ice samples were prepared for isotope dilution (ID) under clean laboratory conditions (see Pyle et al., 2017, for full details). Aliquots of acidified seawater (samples and reference standards) were spiked gravimetrically with a ^{135}Ba-enriched solution (10 μg/ mL ^{135}Ba, Inorganic Ventures, Christiansburg, VA, USA, gravimetrically diluted to a working spike solution with a concentration of approximately 100 nM Ba using 3% Romil UpA HNO$_3$) to achieve a ^{138}Ba/^{135}Ba ratio of 0.65 to 1. The volumes of sample (or standard) and spike solution were determined gravimetrically, and were varied according to the estimated seawater [Ba] in order to keep the spike-to-sample ratio at approximate unity to minimize error magnification.

Spiked samples were left to equilibrate overnight, and were vortexed prior to analysis. All samples and standards were analyzed using inductively coupled plasma mass spectrometry (Bristol Isotope Group, Thermo Element 2). Barium isotopes ^{135}Ba, ^{137}Ba, and ^{138}Ba were measured in low resolution using an SEM detector in counting mode. ^{137}Ba was measured to monitor for interferences on ^{135}Ba and ^{38}Ba. The precise isotopic composition of the spike solution was determined by calibration, utilizing a reverse-ID of blended solutions containing a mixture of the spike solution and a Ba-natural standard from High Purity Standards. The spiked samples and standards were diluted typically 20-fold with 3% Romil UpA HNO$_3$, although the dilution factor depended on the original salinity. Matrix effects as a result of the seawater salts were assessed by routinely analyzing two solutions of dilute seawater standard NASS-6 alongside a 1 ppb Ba-natural standard solution (High Purity Standards): the first NASS-6 solution was diluted 20 times in 3% HNO$_3$, and was used to correct the intensity signal of the second NASS-6 solution, which was diluted 20 times in the 1 ppb Ba-natural standard. The depression or amplification of the "true" signal as a result of the dilute seawater matrix was calculated using the difference in signal intensity between the corrected second NASS-6 solution and the 1ppb Ba-natural standard. This correction varied between runs, but typically resulted in a 20% modification of the blank on both ^{135}Ba and ^{138}Ba, and did not impact the isotopic ratio significantly. A mass bias correction coefficient (typically 2%) was calculated using the deviation of the second NASS-6 solution ^{138}Ba/^{135}Ba ratio from the average natural ratio of ^{138}Ba/^{135}Ba (10.88). The final concentration was calculated using equation (1) (Dickin, 1995):

$$Conc_{sample} = Conc_{spike} \times \frac{m_{spike}}{m_{sample}} \times \left(\frac{R_{spike} - KR_{sample}}{KR_{sample} - R_{natural\ standard}} \right) \times \frac{f_{spike}}{f_{natural\ standard}} \quad (1)$$

Where $Conc_{sample}$ is the sample [Ba]; $Conc_{spike}$ is the spike [Ba]; m is the mass of sample, spike, or natural standard; R is the ratio of ^{138}Ba/^{135}Ba in sample, spike, or natural standard; f is the abundance of ^{135}Ba in spike or natural standard; and K is mass bias correction coefficient for dilute seawater (ratio of literature to measured ratios in dilute seawater). Uncertainties were fully propagated and were typically less than 0.1%. Duplicates were run for every sample, and agreed typically within 0.5%. Reference seawater standards were run routinely to assess precision and accuracy: NASS-6 ([Ba] = 46.9 nmol/kg or 48.1 nM assuming a density of 1.025 kg/L, ±0.9%) and SO ([Ba] = 71.6 nmol/kg or 73.4 nM assuming a density of 1.025 kg/L, ±0.7%), agreeing well with previous studies and other laboratories (Pyle et al., 2017).

Seawater samples were analyzed for oxygen isotope ratios at the British Geological Survey. Oxygen isotope (δ^{18}O) measurements were made using the CO$_2$ equilibration method with an Isoprime 100 mass

spectrometer plus Aquaprep device. Isotope measurements used internal standards calibrated against the international standards VSMOW2 and VSLAP2. Errors are typically $<0.05‰$ for $\delta^{18}O$. Results were reported in standard $\delta^{18}O$ notation (equation (2)), with reference to a standard (Vienna Standard Mean Ocean Water [VSMOW]). Salinity measurements were carried out on board using a Guildline Portasal salinometer, with a typical uncertainty of ±0.003 (Dodd et al., 2017; Meyer et al., 2017b).

$$\delta^{18}O_{sw} = \left\{ \frac{\left(\frac{^{18}O}{^{16}O}\right)_{sample}}{\left(\frac{^{18}O}{^{16}O}\right)_{VSMOW}} - 1 \right\} \cdot 1000 \qquad (2)$$

Details of nutrient and Chl a analyses and uncertainties are detailed in (Assmy et al., 2017). Briefly, nutrient analysis was carried out spectrophotometrically using an adapted Scalar autoanalyzer, and pigments were analyzed on board fluorometrically. Seawater A_T was measured by potentiometric titration with 0.1 N hydrochloric acid using a Versatile Instrument for the Determination of Titration Alkalinity (VINDTA 3S, Marianda, Germany), and accuracy was assessed using analyses of Certified Reference Materials (see Fransson et al., 2017 for details). A_T in melted sea ice samples were analyzed using potentiometric titration with 0.05 N hydrochloric acid at the Institute of Marine Research (IMR), Tromsoe, Norway, using method described in detail by Fransson et al. (2015).

3. Results

3.1. Seawater Barium Measurements

Seawater [Ba] values range from 38.4 to 51.3 nmol/kg, and exhibit relatively low variability and absolute values compared to previous Arctic studies (Abrahamsen et al., 2009; Dodd et al., 2009; Thomas et al., 2011). Despite this low variability, the [Ba] profiles still show characteristic enrichment at depth, with some subsurface peaks above the halocline (Figure 2).

[Ba] showed significant correlations with salinity, A_T, $\delta^{18}O_w$, nitrate, and—most significantly—silicic acid (Table 1). Separate regression analysis for the winter and spring sampling sites may provide further insight, given the very different environmental conditions relating to the water depth, depth of AW, MLD, and biological activity of the two regimes. Multivariate linear analysis of the seawater samples prior to the late-May algal bloom (before 26 May 2015) indicates that [Ba] can be predicted using silicic acid alone ($p < 0.001$, n = 124), with little significance added from A_T and $\delta^{18}O_w$. However, a similar statistical analysis of the samples after to the late-May algal bloom (post 26 May 2015) reveals that [Ba] can be predicted instead using salinity ($p = 0.008$, n = 21) and nitrate ($p = 0.044$) rather than silicic acid ($p > 0.05$).

Alternatively, we can use Principal Component Analysis (PCA) to transform the complex, multiparameter data set to a smaller number of axes, in order to investigate the links between the different parameters (Figure 3). PCA was conducted using a covariance matrix after data normalization for "shallow" ($<50m$) and "deep" ($>50m$) waters. Chi-squared testing showed that the eigenvalues were significantly different in each case.

For the shallow samples, the eigenvalues for PC1, PC2, and PC3 represent a cumulative 73% of the covariance matrix. PC1 has a strong loading with parameters such as date, $\delta^{18}O_w$, nitrate, and silicic acid (which show high intercorrelation), with significant loading with pressure, temperature, and salinity, suggesting this is a strong seasonal signal. PC2 has a strong loading with A_T and—again—with significant loading with pressure, temperature, and salinity. However, [Ba] shows no significant loading with A_T, or nutrients on these axes. PC3 has a strong loading with [Ba], a significant loading with salinity, but no other significant loadings. There are significantly different component scores between the winter (January–March) and summer (April–June) samples for PC1 (Mann-Whitney U tests: PC1 $p < 0.001$) but not for either PC2 or PC3.

For the deep waters, the eigenvalues for PC1 and PC2 represent a cumulative 72% of the covariance matrix (Figure 3). PC1 and PC2 both have significant loadings from all the key environmental parameters, with potential intercorrelation between [Ba], silicic acid, and pressure. Furthermore, there are significantly different component scores between the winter (January–March) and summer (April–June) samples (Mann-Whitney U tests: PC1 $p = 0.029$; PC2 $p < 0.001$).
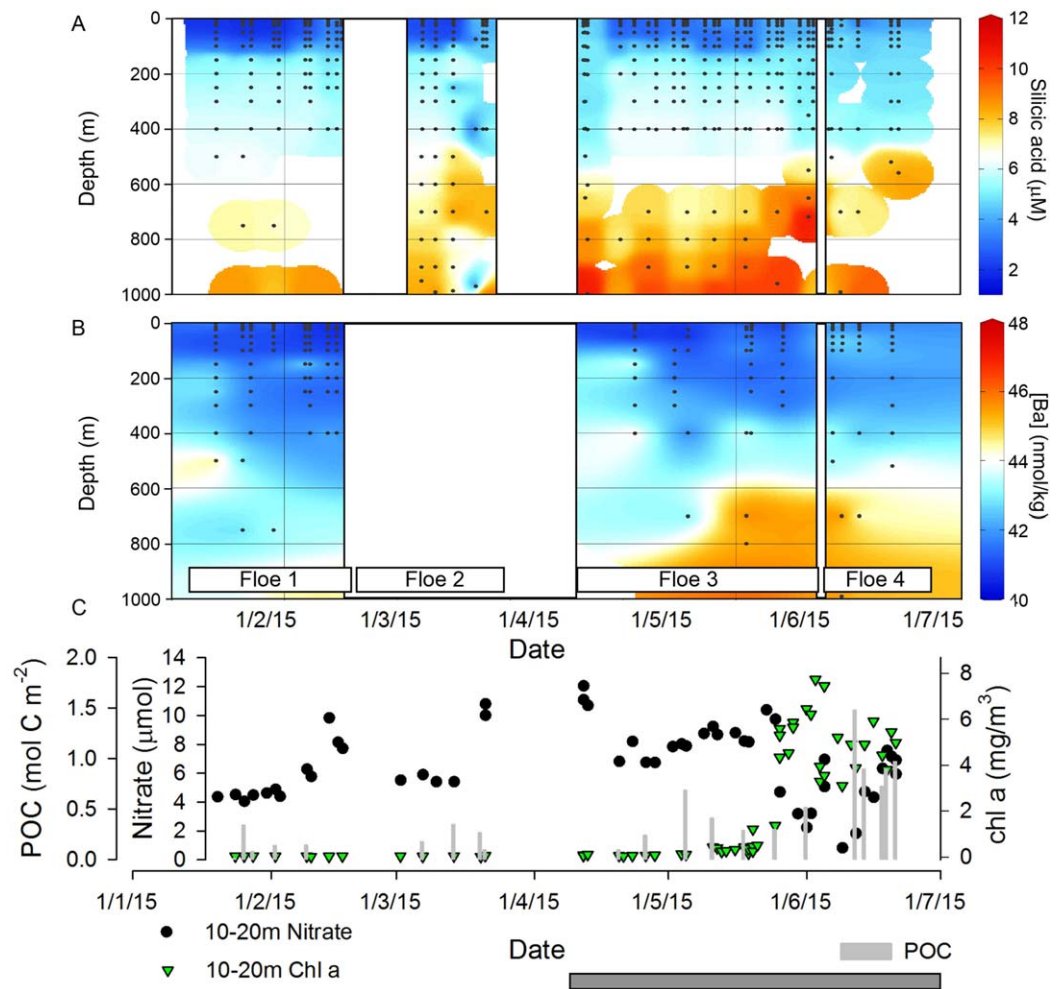
Figure 2. (a) Silicic acid and (b) [Ba] for the N-ICE sampling period, for the top 1000 m. (c) Nitrate and chlorophyll a (Chl *a*) concentrations for samples taken from 10 to 20 m water depth, and particulate organic carbon (POC) integrated over the top 100 m, over the same period when data are available. Floe numbers are marked in white boxes. Dark grey bar shows period when sampling over the continental shelf. With data from Assmy et al. (2016) and Dodd et al. (2017). Plots made using Ocean Data View v.4 and Sigmaplot v. 13.0.

3.1.1. Barite Saturation Indices in Seawater

Barium saturation indices were estimated following Monnin (1999) and Thomas et al. (2011) using the following equation:

$$SI = \frac{Q}{K_{sp}} = \frac{m_{Ba(aq)} \cdot m_{SO_4(aq)} \cdot \gamma^2_{BaSO_4(aq)}}{K_{sp}} \qquad (3)$$

Table 1
Linear Correlation (Pearson Product Moment Coefficients) Between [Ba] and Other Parameters for Seawater Samples for the Whole Data Set

Parameter	R	p	N
Temperature	0.18	0.013	180
Salinity	0.31	<0.001	180
$\delta^{18}O_w$	0.43	<0.001	180
Nitrate	0.48	<0.001	174
Silicic acid	0.68	<0.001	177
A_T	0.30	<0.001	151

Note. Calculated using SigmaPlot v. 13.0.

Where *m* denotes the molality of the species in aqueous form, K_{sp} is the solubility product, γ is the total (or stoichiometric) mean activity coefficient of aqueous barium sulfate (for the general conditions here the following assumptions were made: log $K_{sp} = -10.482$, $\gamma = 0.128$ kg/mol given water temperatures of $1 \pm 2°C$, Monnin, 1999), and Q is the ion activity product of aqueous barium sulfate. The molarity of sulfate was calculated assuming seawater concentrations of 28.23 m*M* at a standard salinity of 35. The molality values for sulfate were converted from molarity using seawater density calculated from temperature, salinity, and pressure measurements from the CTD. The calculations suggest the whole water column is always
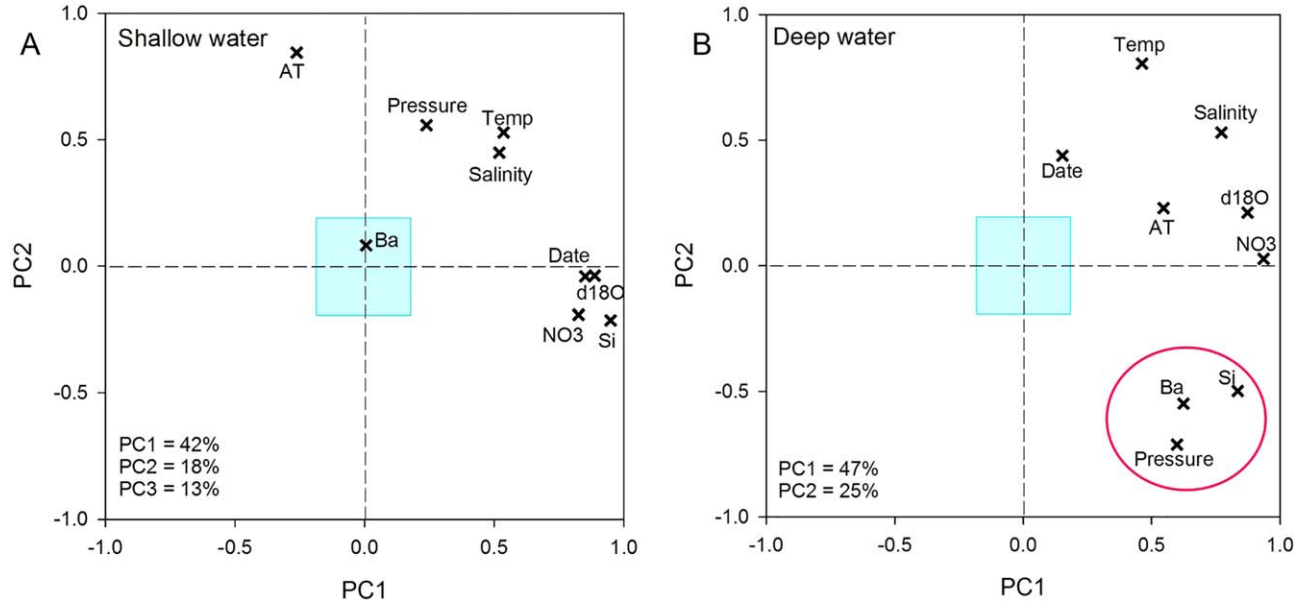
Figure 3. PCA analysis for the environmental parameters measure for (a) shallow water (<50 m) and (b) deep water (>50 m). Clustered variables indicate strong intercorrelation. Nonsignificant variables (values between ±0.2) are highlighted in the cyan boxes. The percentages show how much each component is responsible for the variation in the data set. Red circle highlights relationship between deep water silicic acid and [Ba]. PCA analysis carried out using SigmaPlot v. 13.0.

undersaturated with respect to barite (saturation index 0.5–0.7); any barite formed in the water column must be doing so associated with organic matter and biological production (e.g., Bertram & Cowen, 1997; Collier & Edmond, 1984; Ganeshram et al., 2003; González-Munoz et al., 2003; Paytan & Kastner, 1996).

3.2. Sea-Ice Barium Measurements

Sea-ice section [Ba] values were highly variable and ranged from 5.8 to 79.3 nmol/kg. The relationships between [Ba], salinity, $\delta^{18}O_w$, and nutrients in the sea-ice were also highly variable, and likely related to the structure and of the sea-ice, and whether rafting had occurred (Figure 4). Sea-ice [Ba] did not show significant correlations with salinity, A_T, $\delta^{18}O_w$, or nitrate, and a weakly significant relationship with silicic acid (Table 2). Multivariate linear analysis also indicates only a weakly significant correlation exists between [Ba] and silicic acid ($p \sim 0.02$), and salinity ($p \sim 0.01$).

3.3. Freshwater Decomposition Analysis and Barium Deficiency

The proportion of freshwater fluxes can be calculated from the measured seawater parameters (salinity, A_T, and $\delta^{18}O_w$) using mass balance equations assuming characteristic end-member values for sea-ice, meteoric water, and AW. We calculated the input of the different freshwater sources using two different approaches, using the salinity measurements and either the A_T or $\delta^{18}O_w$ measurements and end-member values in Table 3 to solve equations (4), (5) and either (6) or (7), respectively (Abrahamsen et al., 2009; Cooper et al., 2008; Dodd et al., 2009; Macdonald et al., 1999; Meredith et al., 2001, 2008; Taylor et al., 2003; Thomas et al., 2011).

$$f_{SI} + f_{MW} + f_{SW} = 1 \tag{4}$$

$$(S_{SI} * f_{SI}) + (S_{MW} * f_{MW}) + (S_{SW} * f_{SW}) = S \tag{5}$$

$$(\delta_{SI} * f_{SI}) + (\delta_{MW} * f_{MW}) + (\delta_{SW} * f_{SW}) = \delta \tag{6}$$

$$(A_{TSI} * f_{SI}) + (A_{TMW} * f_{MW}) + (A_{TSW} * f_{SW}) = A_T \tag{7}$$

where f_{SI}, f_{MW}, and f_{AW} are the fractions of sea-ice melt, meteoric water, and seawater end-members, respectively, that we seek to determine; S_{SI}, S_{MW}, and S_{SW} are the respective salinities of the end members; δ_{SI}, δ_{MW}, and δ_{SW} are their corresponding $\delta^{18}O_w$ values; and A_{TSI}, A_{TMW}, and A_{TSW} are their corresponding alkalinities (Table 3). We assessed the meteoric end-member using data from the upper 400 m of the water column. In the case of the seawater end-member, we plotted A_T versus S to obtain a linear fit (equation (8)).
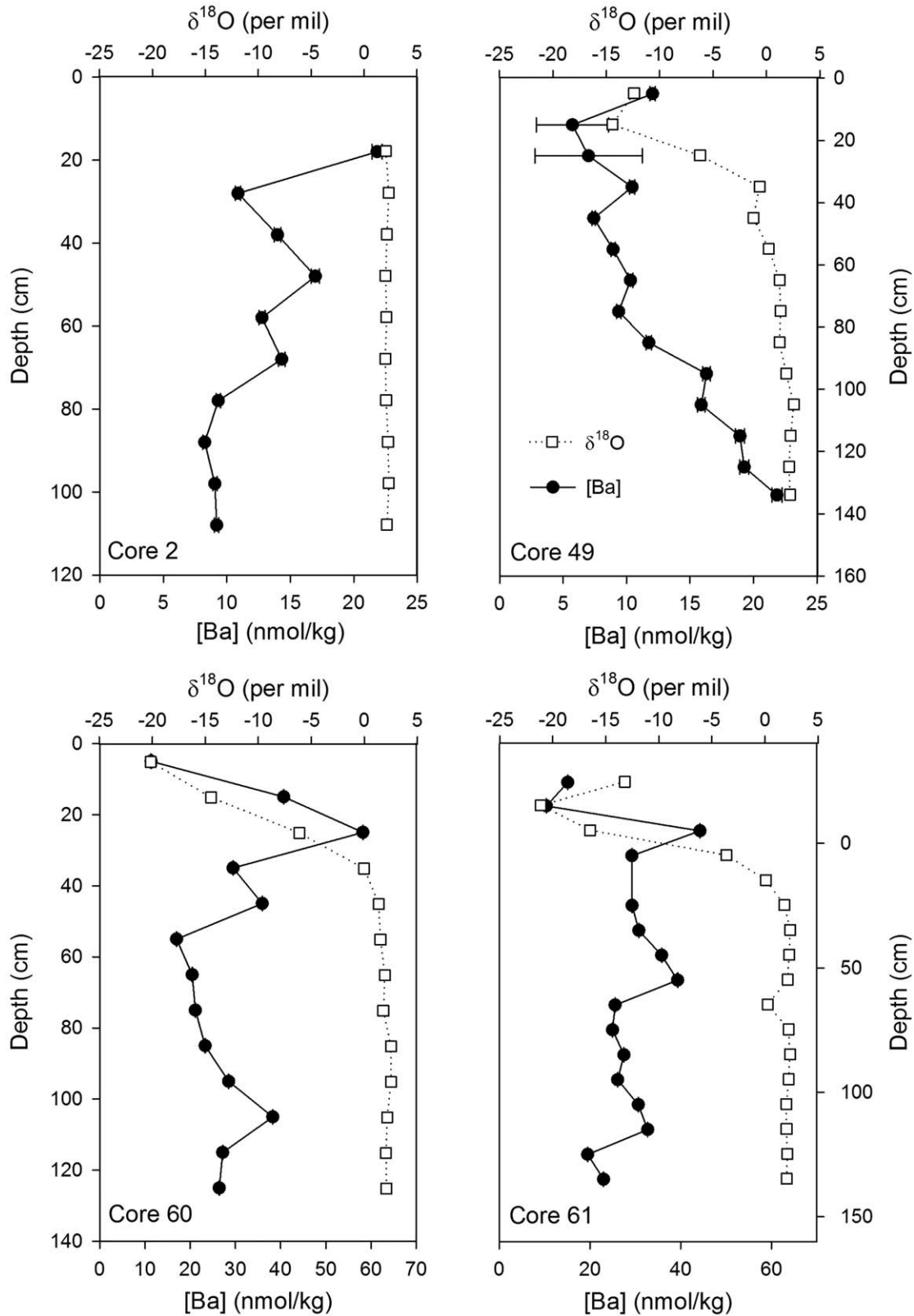
Figure 4. Examples of ice-core profiles of [Ba] in nmol/kg and $\delta^{18}O$ for N-ICE2015. Salinity is highly variable in the cores due to the presence of brine pockets (See supporting information), $\delta^{18}O$ is a stronger indication of precipitation because of the similar isotope compositions of brine and ice.

Table 2
Linear Correlation (Pearson Product Moment Coefficients) Between [Ba] and Other Parameters for Sea-Ice Samples

Parameter	R	p	n
Silicic acid	0.31	0.02	62
Nitrate	−0.03	0.80	62
Salinity	0.17	0.09	96
$\delta^{18}O_w$	−0.05	0.65	96

Note. Calculated using SigmaPlot v. 13.0.

Table 3
End-Member Values Used for the Freshwater Decomposition Analysis

	AT (μmol/kg)	Salinity	$\delta^{18}O_w$ (‰)
Meteoric water	390[a]	0[b]	−20[b]
Sea-ice melt	370[a]	5.8[a]	+2.1[a]
Seawater	2312[a]	35.06[a]	+0.4[a]

[a]From N-ICE data set (see text for explanation). [b]$\delta^{18}O_w$ values from Thomas et al. (2011) and Chierici et al. (2011).

$$A_T = 54.82 * S + 390 \tag{8}$$

Given that the highest salinity was 35.06 this results in a seawater end-member A_T of 2312 μmol/kg (Fransson et al., 2001). Mean sea-ice salinity was calculated (range salinity of 0–15), truncating values at 15. Sea-ice A_T (370 μmol/kg) at mean sea-ice salinity (5.8) was calculated obtained from sea-ice A_T versus sea-ice salinity linear relation $A_T = 63.84 *S$ (r2 = 0.97; N = 69) based on N-ICE2015 A_T data, where outliers from the regression line were removed due to nonlinear processes such as calcium carbonate precipitation/dissolution, affecting A_T (Fransson et al., 2013, 2017). For comparison, assuming a simple mixing line with seawater without nonlinear sea-ice processes, A_T of 382 μmol/kg was obtained (Chierici et al., 2011; Thomas et al., 2011); using this calculated value in the mass balance calculations yields the same results within uncertainty as the observed value (supporting information). Sea-ice $\delta^{18}O$ was taken as the maximum value in the data set; seawater $\delta^{18}O$ was taken as the value the water column data converges to at depth. The meteoric water inputs represent the greatest uncertainties in these mass balance calculations, as there are no direct measurements and a wide range of seasonality (leading to a range in $\delta^{18}O_w$) for the nonmarine freshwaters. Sensitivity testing, using a range of possible A_T and $\delta^{18}O$ values for the end-member compositions, shows that the uncertainties in our calculated freshwater contributions are unlikely to be significant relative to the water column variability (supporting information). Furthermore, these end-member uncertainties are likely to be systematic and do not necessarily impact the patterns and trends observed in the data (Pyle et al., 2017).

Using the reconstructed freshwater inputs, we then calculated the expected [Ba] ([Ba]$_{pred}$) assuming the SW and Eurasian rivers contribute 49 and 120 nmol/kg [Ba], respectively, assuming a river water density of 1kg/L (Dodd et al., 2009), and, therefore, a barium "deficit" ([Ba]$_{Def}$):

$$[Ba]_{Pred} = \%SW * 49 + \%MET * 120 \tag{9}$$

$$[Ba]_{Def} = [Ba]_{pred} - [Ba]_o \tag{10}$$

Where [Ba]$_o$ is the measured barium concentration. The resulting [Ba]$_{Def}$ values based on reconstructed %SW and %MET from the A_T and $\delta^{18}O_w$ mass balances are significantly correlated, and fall approximately on a 1:1 line (Figure 5), although the $\delta^{18}O_w$-based reconstructions bias toward higher deficits. An example of the time series of [Ba]$_{Def}$ based on alkalinity is shown in Figure 6.

Last, we converted the [Ba]$_{Def}$ into a carbon flux, assuming a C_{org}:Ba$_{xs}$ value of 225 g C (g Ba)$^{-1}$ (Thomas et al., 2011). However, assuming that there is a consistent link between the "barium deficit" and carbon uptake is problematic; the reconstructed carbon fluxes are very similar for the winter and summer samples, for example using the A_T-based reconstruction results in all profiles yielding approximately 0.4–2.3 mol C m^{-2}. While these values are the same order of magnitude as the measured integrated POC levels in the water column (Figure 2), they do not reflect the temporal variation in biological standing stocks.

Figure 5. Comparison of the reconstructed barium "deficits" from freshwater component reconstructions from salinity and either $\delta^{18}O_w$ or A_T. See text (equations (5)–(9)) for details. The line shows a 1:1 relationship. There is generally good agreement between the two methods (Pearson Product Moment correlation coefficient R = 0.54, $p < 0.001$), although the $\delta^{18}O_w$-based reconstructions bias toward significantly higher deficits (failed Shapiro-Wilk Normality Test ($p < 0.05$); Mann-Whitney U Statistic = 7378, T = 26899, n = 151, $p < 0.001$). Statistical analysis carried out using SigmaPlot v. 13.0.

4. Discussion

The water column [Ba] measurements, statistical analysis, and freshwater calculations point toward an uptake of barium via nonconservative processes that are active in seawater and sea-ice in winter as well
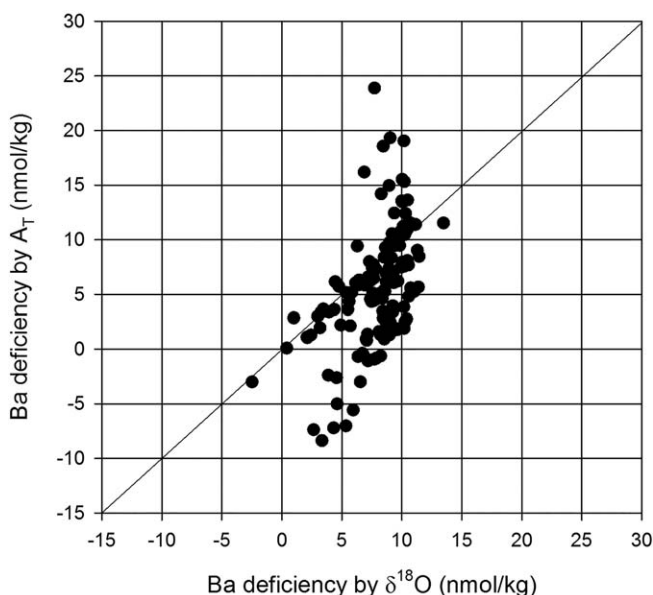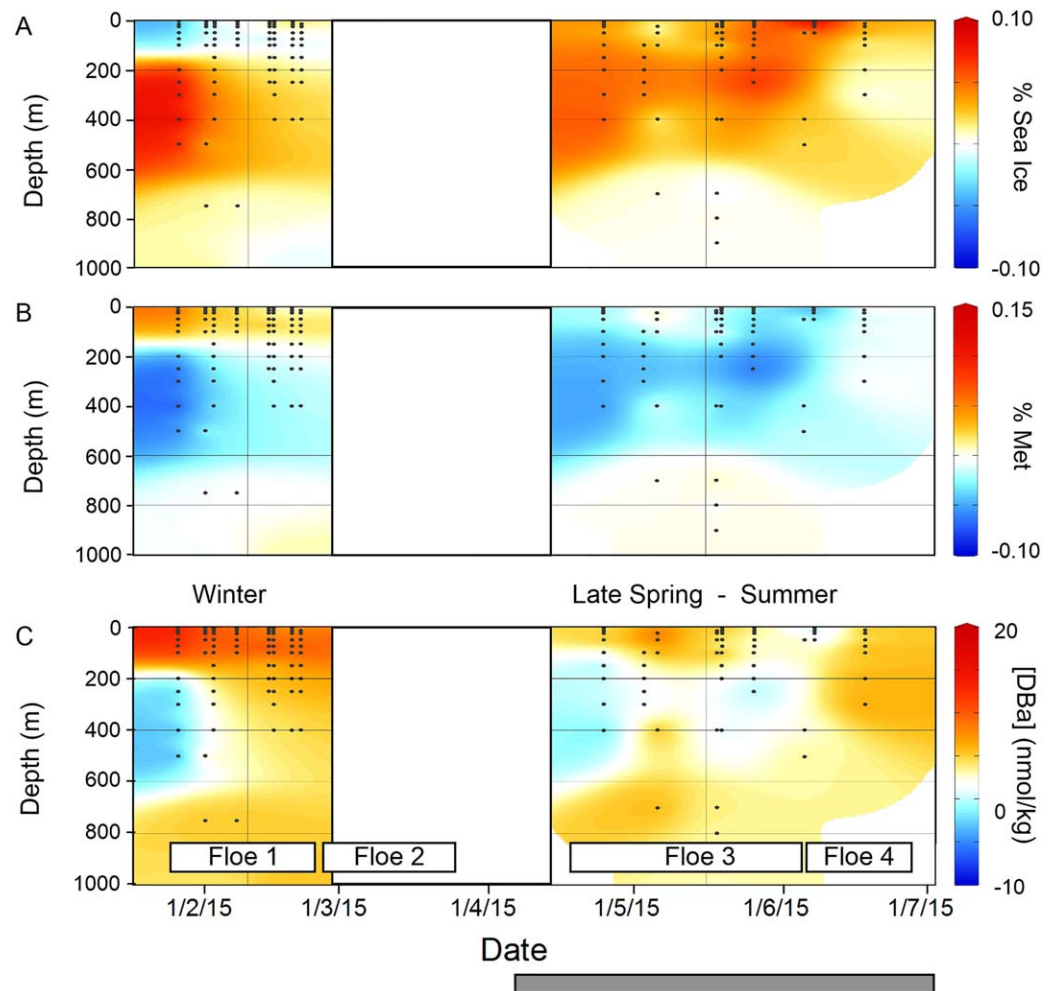
Figure 6. Time series plots of the percentage contribution of freshwater from (a) sea-ice, and (b) meteoric water; (c) the calculated barium "deficit." All based on A_T reconstructions; see text for details. Dark grey bar shows period when sampling over the continental shelf. Floe numbers are marked in white boxes. Plots made using Ocean Data View v.4.

as during the biologically productive summer months. There are a series of questions that arise from these findings: first, are the freshwater component mass-balance calculations reliable? And, second, if so, what are the processes that result in a strong $[Ba]_{Def}$ in the water column in winter and early summer, before the spring bloom? Here, we will assess the assumptions made when calculating $[Ba]_{Def}$, and the possible processes that can explain the "seasonal" patterns that are observed.

4.1. Assessing the Freshwater Reconstruction

The method of separating freshwater inputs using a combination of salinity measurements and either $\delta^{18}O_w$ or A_T is well-established, with—in each case—the resulting derived freshwater fractions reported here as percentages with typical errors of <1% on point values that can be attributed to variations in end-members (i.e., the sea-ice, meteoric, and oceanic compositions) (e.g., Meredith et al., 2013, and sensitivity testing—see supporting information; Pyle et al., 2017). If these end-members are invariable in time and space, then these uncertainties will be systematic across the whole data set. The generally good agreement when carrying out the calculations using either $\delta^{18}O_w$ or A_T suggests that the reconstructed freshwater components are reliable, at least for determining relative spatial and temporal changes. However, if these end-members are temporally or spatially variable, then there could be some bias introduced into the calculations. A further problem arises when subsequently calculating the $[Ba]_{Def}$ from this method; the calculation assumes that there is one, uniform riverine composition, and does not take into consideration seasonal or spatial changes in river input.

4.2. The Behavior of [Ba] in the Water Column

The statistical analysis of the N-ICE2015 water column data set reveals a complex relationship between [Ba] and other environmental parameters, which may impact on the utility of dissolved barium as a tracer of water masses. In deeper waters, there is likely a link between [Ba] and the supply of underlying AW: for samples >50 m water depth there is some clustering with [Ba] and other parameters in the Principal Component Analysis (PCA) plots (Figure 3), suggesting some intercorrelation with silicic acid and pressure (i.e., depth). However, the results of our multivariate analyses seem to suggest that [Ba] is influenced by different factors at different times of year. This likely reflects the different oceanographic conditions rather than temporal changes *per se*, with "true" Arctic water masses in the winter, compared to the location over the Yermak Plateau occupied in the summer, where there is permanent AW incursion at depth.

In contrast to deeper waters, our PCA analysis showed that surface water [Ba] (<50 m) has little relationship to any parameter except salinity. PC1 revealed a strong seasonal signal, which likely reflects variations in the mixed layer depth (MLD) and the strong variability in meltwater in surface waters. Although 50 m was selected as an approximate average MLD for the cut-off between "shallow" and "deep" for the purposes of the PCA analysis, MLDs were much shallower in the late summer, with AW found up to the surface during some periods later in the drift expedition (Meyer et al., 2017b). However, this change in MLD does not drive the variability in [Ba] observed in the surface waters, as the PCA plots do not reveal any clustering between [Ba] and other parameters or any significant loading of [Ba] on PC1 (Figure 3). Instead, [Ba] only significantly contributes to the loading of PC3, which also has some contribution from temperature and salinity and—weakly—from A_T and pressure.

Our results suggest that it is challenging to associate [Ba] straightforwardly with another environmental parameter in the near surface ocean—except potentially salinity most likely as a result of riverine inputs—and that there is no clear difference in the behavior of surface [Ba] between the winter and summer months. It is possible that there is a further environmental parameter that impacts [Ba], which was not included in the PCA, or that the variability in [Ba] was too low to detect intercorrelations with other parameters effectively.

4.3. Mechanisms Behind the Seasonal Changes in Ba Deficiency in Seawater

The seawater profiles illustrate that there are potential barium "deficits" in the water column throughout the winter and spring that are not observed strongly in the summer, regardless of how the freshwater input is calculated. The spring barium deficit occurred in late April–May, and is likely a result of Ba uptake associated with biological material produced during the early under-ice production when moderate Chl *a* concentrations were detected at approximately 40 m (Assmy et al., 2017). However, Chl *a* and POC levels in winter were low and biological production is unlikely to have formed an efficient sink of barium.

Assuming the $[Ba]_{Def}$ calculations are reflecting the water column conditions, there are several possible explanations for this variability in barium uptake that relate to conditions external to the water column system. First, processes within sea-ice—either during its earlier formation or during its later development and snow-ice transitions—could cause nonconservative behavior of barium that leaves a depleted surface water signal behind (see section 4.4). Evidence for a sea-ice influence comes from a comparison between the calculated $[Ba]_{Def}$ and the meltwater mass balance calculations in winter. The strong barium deficit in winter seems to correspond to a higher meteoric water input, which is unexpected if riverine inputs are assumed to be the major supplier of dissolved Ba. However, there is also a negative contribution to freshwater from sea-ice, indicative that freshwater had been lost from that particular water mass as a result of sea-ice formation prior to sampling (Figure 6).

Second, barium could be taken up by association with slowly remineralizing, old organic matter that remains in the water column from the previous summer or autumn, rather than new production (Reigstad et al., 2002). The N-ICE2015 observations reveal that there was POC present in the water column during winter, despite very low Chl *a* concentrations in the near surface water (Figure 2), suggesting that there could have been old POC remaining from the previous summer (Assmy et al., 2017; Olsen et al., 2017). The older, more recalcitrant organic matter could remain in the water column for a sufficient amount of time to develop barite saturation within microenvironments.

Third, there could be variable depletion of [Ba] by association with organic matter, as a result of spatial and temporal differences in phytoplankton community structure. Only a very small proportion of particulate barium in seawater is directly incorporated into biological material (Horner et al., 2015), but is most likely adsorbed or precipitated as barite in microenvironments within the organic matter. Given that there is no fixed stoichiometry between dissolved barium and inorganic nutrients (Collier & Edmond, 1984), it is possible that the capacity for barium uptake is dependent on the properties such as the chemical composition of both skeletal elements and soft parts, cell size, and density. Barium uptake may be greater in diatom-dominated communities compared to the *Phaeocystis*-dominated communities observed during the summer months of N-ICE2015 (Assmy et al., 2017). Furthermore, the dominance of *Phaeocystis* after 26 May could potentially explain why there is a weaker coupling between [Ba] and silicic acid, and a stronger relationship with nitrate, in the later part of the study.

Last, there could be rapid remineralization of barium in near surface waters during the summer due to an enhanced microbial loop resulting from warmer temperatures, changes in sea-ice conditions or proximity to the shelf. Rapid and shallow turnover, with a strong halocline, may result in barium becoming effectively trapped near the surface. This process, again, could also explain why there appears to be a stronger relationship between [Ba] and nitrate in summer, rather than silicic acid, given the former has the shallower remineralization depth. Such changes in remineralization could also be driven by phytoplankton community structure.

The lack of a strong barium deficit in summer may be driven by a number of nonmutually exclusive processes. There could be additional barium inputs near the shelf, as a result of season-dependent meteoric water compositions (Colbert & McManus, 2005; Cooper et al., 2008; Guay & Falkner, 1997, 1998); different AW concentrations due to shelf sediment remobilization or diffusion, especially in suboxic sediments below highly productive regions (McManus et al., 1994); or changes in water mass age or ventilation.

4.4. Sea-Ice Barium: Non-Conservative Behavior or Multiple End-Member Mixing?

Barium in the sea-ice samples did not fall on a simple linear mixing line that would represent conservative dilution by low-[Ba] freshwater (Figure 7), which has been observed for trace elements—including barium—in Antarctic sea-ice (Hendry et al., 2009; Lannuzel et al., 2011). This observation means that either nonconservative processes are active within sea-ice on or that the system cannot be described as simple mixing between two end-members, and sea-ice could be a source or sink of barium that would invalidate the assumptions that form the basis of equation (8).

For nonconservative behavior within sea ice, barium must be removed from or added to solution independently of salinity changes. Sea-salt ions are rejected from the ice crystal lattice as sea ice forms, forming pockets of brine that become trapped in a network within the ice; the trapped, dense brine drains downwards through brine channels under the influence of gravity, typically leaving upper layers of ice fresher (Weeks & Ackley, 1982). The extent of this desalination is determined by the permeability of the sea ice, which in turn is controlled by the structure of the ice itself and its thermodynamic properties, with freezing in brine channels decreasing porosity (Backstrom & Eicken, 2006; Golden et al., 1998). Within these brine channels, barium could be removed from solution into solid phases either by adsorption onto particulates, or through the precipitation of barite. The formation of barite may be promoted in microenvironments associated with the concentration of Ba^{2+} and SO_4^{2-} ions in brine channels released from the decay of organic matter, promoted by a dynamic sea-ice microbial community (Lannuzel et al., 2011; Palmisano & Garrison, 1993; Stroobants et al., 1991). Provided that such barite crystals did not redissolve, this mechanism would remove barium from solution independently of salinity fluctuations. However, if this were the primary mechanism driving the dissociation between [Ba] and salinity (supporting information) that is observed in the Arctic sea ice core samples, a correlation could be expected between [Ba] and the concentrations of dissolved inorganic nutrients (as indicators of productivity), which is not typically observed in these samples.

Barite precipitation may also be able to occur within sea ice without the aid of microbial microenvironments. SO_4^{2-} ions make up approximately 8% of the mass of salt ions in sea water, and it is possible that brine pockets may reach high enough concentrations of barium and sulfate to cause abiotic precipitation of barite.
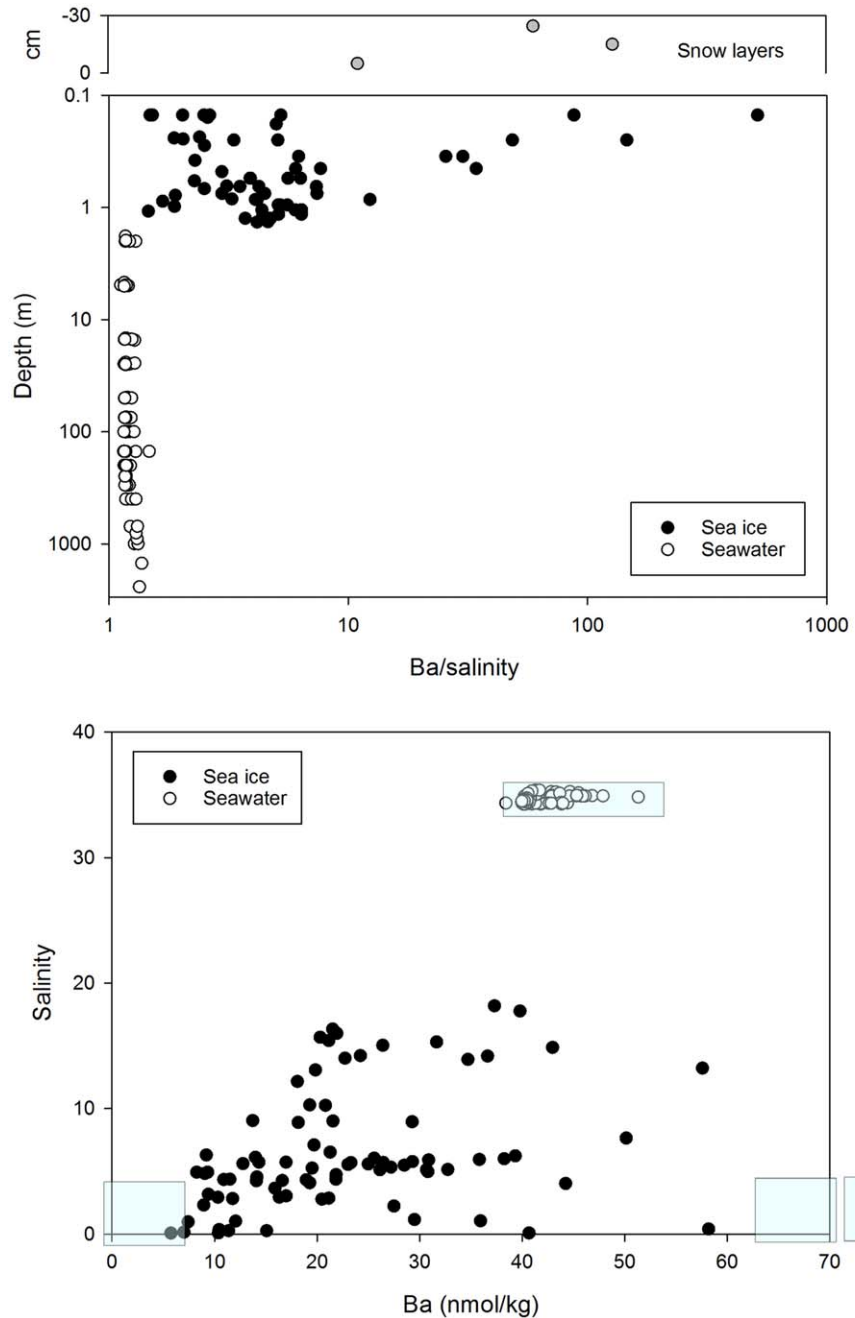
Figure 7. (a) Salinity normalized [Ba] in sea ice and seawater (grey symbols show results for overlying snowpack). (b) Salinity plotted against [Ba] for the same samples; the lack of a simple mixing curve indicates complex mixing behavior with multiple end-members, shown schematically as the blue boxes.

An alternative explanation is that there is an additional input, i.e., a third or higher-order end-member—of the barium within the sea-ice (Figure 7), which could derive from various possible sources. Whilst it appears that seawater quantitatively supplies the [Ba] in Antarctic sea-ice (Lannuzel et al., 2011), is it possible that the higher atmospheric deposition of dust in the northern high latitudes results in a nontrivial contribution of atmospheric barium to Arctic sea-ice? This hypothesis is supported by the relatively high normalized [Ba] content of the snow pack (Figure 7), and could be particularly the case in this study as samples were not filtered on collection.

5. Conclusions

The high-latitude Arctic is a critical region in determining global distributions of heat, carbon, and nutrients through its role in controlling the density of water exported to the North Atlantic and, so, deep-water formation in the Labrador Sea. Freshwater contributions are commonly calculated using geochemical tracers, for use in models that are critical for assessing future oceanographic change. We present new observations that challenge the assumptions surrounding the use of barium as a freshwater tracer of riverine input in the Arctic, showing nonconservative behavior even during periods of low biological productivity, most likely as a result of processes occurring in sea-ice microenvironments. In contrast, in the high productivity summer months, we find surplus near surface barium, despite high standing stocks of organic carbon, perhaps reflecting phytoplankton assemblage changes, or/and rapid internal cycling. Our findings highlight the need to better understand the behavior of barium in high-latitude regions, and further insight will be gained from detailed examination of particulate barium in sea-ice samples, and through barium isotope process studies.

References

Abrahamsen, E. P., Meredith, M. P., Falkner, K. K., Torres-Valdes, S., Leng, M. J., Alkire, M. B., et al. (2009). Tracer-derived freshwater composition of the Siberian continental shelf and slope following the extreme Arctic summer of 2007. *Geophysical Research Letters*, *36*, L07602. https://doi.org/10.1029/2009GL037341

Alexeev, V., Ivanov, V., Kwok, R., & Smedsrud, L. (2013). North Atlantic warming and declining volume of arctic sea ice. *Cryosphere Discussions*, *7*, 245–265.

Assmy, P., Duarte, P., Dujardin, J., Fernandez-Mendez, M., Fransson, A., Hodgson, R., & Wold, A. (2016). *N-ICE2015 water column biogeochemistry*. Tromsø, Norway: Norwegian Polar Institute, Norwegian Polar Institute. https://doi.org/10.21334/npolar.2016.3ebb7f64

Assmy, P., Fernández-Méndez, M., Duarte, P., Meyer, A., Randelhoff, A., Mundy, C. J., et al. (2017). Leads in Arctic pack ice enable early phytoplankton blooms below snow-covered sea ice. *Scientific Reports*, *7*, 40850.

Backstrom, L. G., & Eicken, H. (2006). Capacitance probe measurements of brine volume and bulk salinity in first-year sea ice. *Cold Regions Science and Technology*, *46*, 167–180.

Bates, S. L., Hendry, K. R., Pryer, H. V., Kinsley, C. W., Pyle, K. M., Woodward, E. M. S., et al. (2017). Barium isotopes reveal role of ocean circulation on barium cycling in the Atlantic. *Geochimica Et Cosmochimica Acta*, *204*, 286–299.

Bertram, M. A., & Cowen, J. P. (1997). Morphological and compositional evidence for biotic precipitation of marine barite. *Journal of Marine Research*, *55*, 577–593.

Cardinal, D., Savoye, N., Trull, T. W., André, L., Kopczynska, E. E., & Dehairs, F. (2005). Variations of carbon remineralization in the Southern Ocean illustrated by the Ba xs proxy. *Deep Sea Research Part I: Oceanographic Research Papers*, *52*, 355–370.

Chierici, M., Fransson, A., Lansard, B., Miller, L. A., Mucci, A., Shadwick, E., et al. (2011). Impact of biogeochemical processes and environmental factors on the calcium carbonate saturation state in the Circumpolar Flaw Lead in the Amundsen Gulf, Arctic Ocean. *Journal of Geophysical Research*, *116*, C00G09. https://doi.org/10.1029/2011JC007184

Colbert, D., & McManus, J. (2005). Importance of seasonal variability and coastal processes on estuarine manganese and barium cycling in a Pacific Northwest estuary. *Continental Shelf Research*, *25*, 1395–1414.

Collier, R., & Edmond, J. (1984). The trace element geochemistry of marine biogenic particulate matter. *Progress in Oceanography*, *13*, 113–199.

Cooper, L. W., McClelland, J. W., Holmes, R. M., Raymond, P. A., Gibson, J., Guay, C. K., et al. (2008). Flow-weighted values of runoff tracers (δ18O, DOC, Ba, alkalinity) from the six largest Arctic rivers. *Geophysical Research Letters*, *35*, L18606. https://doi.org/10.1029/2008GL035007

Dehairs, F., Stroobants, N., & Goeyens, L. (1991). Suspended barite as a tracer of biological activity in the Southern Ocean. *Marine Chemistry*, *35*, 399–410.

Dickin, A. P. (1995). *Radiogenic isotope geology*. Cambridge, UK: Cambridge University Press.

Dodd, P., Meyer, A., Koenig, Z., Cooper, A., Smedsrud, L. H., Muilwijk, M., et al. (2017). N-ICE2015 ship-based conductivity-temperature-depth (CTD) data. Tromsø, Norway: Norwegian Polar Institute. https://doi.org/10.21334/npolar.2017.92262a9c

Dodd, P. A., Heywood, K. J., Meredith, M. P., Naveira-Garabato, A. C., Marca, A. D., & Falkner, K. K. (2009). Sources and fate of freshwater exported in the East Greenland Current. *Geophysical Research Letters*, *36*, L19608. https://doi.org/10.1029/2009GL039663

Eagle, M., Paytan, A., Arrigo, K. R., van Dijken, G. L., & Murray, R. W. (2003). A comparison between excess barium and barite as indicators of carbon export. *Paleoceanography*, *18*(3), 1021.

Fransson, A., Chierici, M., Abrahamsson, K., Andersson, M., Granfors, A., Gårdfeldt, K., et al. (2015). CO 2-system development in young sea ice and CO 2 gas exchange at the ice/air interface mediated by brine and frost flowers in Kongsfjorden, Spitsbergen. *Annals of Glaciology*, *56*, 245–257.

Fransson, A., Chierici, M., Anderson, L. G., Bussmann, I., Kattner, G., Jones, E. P., et al. (2001). The importance of shelf processes for the modification of chemical constituents in the waters of the Eurasian Arctic Ocean: Implication for carbon fluxes. *Continental Shelf Research*, *21*, 225–242.

Fransson, A., Chierici, M., Miller, L. A., Carnat, G., Shadwick, E., Thomas, H., et al. (2013). Impact of sea-ice processes on the carbonate system and ocean acidification at the ice-water interface of the Amundsen Gulf, Arctic Ocean. *Journal of Geophysical Research: Oceans*, *118*, 7001–7023. https://doi.org/10.1002/2013JC009164

Fransson, A., Chierici, M., Skjelvan, I., Olsen, A., Assmy, P., Peterson, A. K., et al. (2017). Effects of sea-ice and biogeochemical processes and storms on under-ice water fCO2 during the winter-spring transition in the high Arctic Ocean: Implications for sea-air CO2 fluxes. *Journal of Geophysical Research: Oceans*, *122*, 5566–5587. https://doi.org/10.1002/2016JC012478

Ganeshram, R. S., Francois, R., Commeau, J., & Brown-Leger, S. L. (2003). An experimental investigation of barite formation in seawater. *Geochimica Et Cosmochimica Acta*, *67*, 2599–2605.

Golden, K. M., Ackley, S. F., & Lytle, V. I. (1998). The percolation phase transition in sea ice. *Science*, *282*, 2238–2241.

González-Munoz, M. T., Fernández-Luque, B., Martínez-Ruiz, F., Chekroun, K. B., Arias, J. M., Rodríguez-Gallego, M., et al. (2003). Precipitation of barite by Myxococcus xanthus: Possible implications for the biogeochemical cycle of barium. *Applied and Environmental Microbiology*, *69*, 5722–5725.

Granskog, M. A., Assmy, P., Gerland, S., Spreen, G., Steen, H., & Smedsrud, L. H. (2016). Arctic research on thin ice: Consequences of Arctic sea ice loss. *EOS Transactions of American Geophysical Union*, *97*(5), 22–26.

Guay, C. K., & Falkner, K. K. (1997). Barium as a tracer of Arctic halocline and river waters. *Deep Sea Research Part II: Topical Studies in Oceanography*, *44*, 1543–1569.

Guay, C. K., & Falkner, K. K. (1998). A survey of dissolved barium in the estuaries of major Arctic rivers and adjacent seas. *Continental Shelf Research*, *18*, 859–882.

Hendry, K. R., Rickaby, R. E. M., de Hoog, J. C. M., Weston, K., & Rehkamper, M. (2009). The cadmium-phosphate relationship in brine: Biological versus physical control over micronutrients in sea ice environments. *Antarctic Science*, *22*, 1–18. https://doi.org/10.1017/S0954102009990381

Horner, T. J., Kinsley, C. W., & Nielsen, S. G. (2015). Barium-isotopic fractionation in seawater mediated by barite cycling and oceanic circulation. *Earth and Planetary Science Letters*, *430*, 511–522.

Hsieh, Y.-T., & Henderson, G. M. (2017). Barium stable isotopes in the global ocean: Tracer of Ba inputs and utilization. *Earth and Planetary Science Letters*, *473*, 269–278.

Itkin, P., Spreen, G., Cheng, B., Doble, M., Girard-Ardhuin, F., Haapala, J., et l. (2017). Thin ice and storms: Sea ice deformation from buoy arrays deployed during N-ICE2015. *Journal of Geophysical Research: Oceans*, *122*, 4661–4674. https://doi.org/10.1002/2016JC012403

Jacquet, S., Dehairs, F., Cardinal, D., Navez, J., & Delille, B. (2005). Barium distribution across the Southern Ocean frontal system in the Crozet–Kerguelen Basin. *Marine Chemistry*, *95*, 149–162.

Jeandel, C., Dupre, B., Lebaron, G., Monnin, C., & Minster, J.-F. (1996). Longitudinal distributions of dissolved barium, silica and alkalinity in the western and southern Indian Ocean. *Deep Sea Research Part I: Oceanographic Research Papers*, *43*, 1–31.

Jullion, L., Jacquet, S., & Tanhua, T. (2017). Untangling biogeochemical processes from the impact of ocean circulation: First insight on the Mediterranean dissolved barium dynamics. *Global Biogeochemical Cycles*, *31*, 1256–1270. https://doi.org/10.1002/2016GB005489

Kauko, H. M., Taskjelle, T., Assmy, P., Pavlov, A. K., Mundy, C., Duarte, P., et al. (2017). Windows in Arctic sea ice: Light transmission and ice algae in a refrozen lead. *Journal of Geophysical Research: Biogeosciences*, *122*, 1486–1505 https://doi.org/10.1002/2016JG003626

Koenig, Z., Provost, C., Villacieros-Robineau, N., Sennéchael, N., & Meyer, A. (2016). Winter ocean-ice interactions under thin sea ice observed by IAOOS platforms during N-ICE2015: Salty surface mixed layer and active basal melt. *Journal of Geophysical Research: Oceans*, *121*, 7898–7916. https://doi.org/10.1002/2016JC012195

Lannuzel, D., Bowie, A. R., van der Merwe, P. C., Townsend, A. T., & Schoemann, V. (2011). Distribution of dissolved and particulate metals in Antarctic sea ice. *Marine Chemistry*, *124*, 134–146.

Macdonald, R., Carmack, E., McLaughlin, F., Falkner, K., & Swift, J. (1999). Connections among ice, runoff and atmospheric forcing in the Beaufort Gyre. *Geophysical Research Letters*, *26*, 2223–2226.

McManus, J., Berelson, W. M., Klinkhammer, G. P., Kilgore, T. E., & Hammond, D. E. (1994). Remobilization of barium in continental margin sediments. *Geochimica Et Cosmochimica Acta*, *58*, 4899–4907.

Meredith, M., Heywood, K., Dennis, P., Goldson, L., White, R., Fahrbach, E., et al. (2001). Freshwater fluxes through the western Fram Strait. *Geophysical Research Letters*, *28*, 1615–1618.

Meredith, M. P., Brandon, M. A., Wallace, M. I., Clarke, A., Leng, M. J., Renfrew, I. A., . . . King, J. C. (2008). Variability in the freshwater balance of northern Marguerite Bay, Antarctic Peninsula: Results from d^{18}O. *Deep Sea Research II: Topical Studies in Oceanography*, *55*, 309–322.

Meredith, M. P., Venables, H. J., Clarke, A., Ducklow, H. W., Erickson, M., Leng, M. J., et al. (2013). The freshwater system west of the Antarctic Peninsula: Spatial and temporal changes. *Journal of Climate*, *26*, 1669–1684.

Meyer, A., Fer, I., Sundfjord, A., & Peterson, A. K. (2017a). Mixing rates and vertical heat fluxes north of Svalbard from Arctic winter to spring. *Journal of Geophysical Research: Oceans*, *122*, 4569–4586. https://doi.org/10.1002/2016JC012441

Meyer, A., Sundfjord, A., Fer, I., Provost, C., Villacieros Robineau, N., Koenig, Z., et al. (2017b). Winter to summer oceanographic observations in the Arctic Ocean north of Svalbard. *Journal of Geophysical Research: Oceans*, *122*, 6218–6237. https://doi.org/10.1002/2016JC012391

Monnin, C. (1999). A thermodynamic model for the solubility of barite and celestite in electrolyte solutions and seawater to 200 C and to 1 kbar. *Chemical Geology*, *153*, 187–209.

Olsen, L. M., Laney, S. R., Duarte, P., Kauko, H. M., Fernández-Méndez, M., Mundy, C. J., et al. (2017). The seeding of ice-algal blooms in Arctic pack ice: The multiyear ice seed repository hypothesis. *Journal of Geophysical Research: Biogeosciences*, *122*, 1529–1548. https://doi.org/10.1002/2016JG003668

Palmisano, A. C., & Garrison, D. L. (1993). Micro-organisms in Antarctic sea-ice. In I. Friedman (Ed.), *Antarctic microbiology*. New York, NY: Wiley-Liss.

Paytan, A., & Kastner, M. (1996). Benthic Ba fluxes in the central Equatorial Pacific, implications for the oceanic Ba cycle. *Earth and Planetary Science Letters*, *142*, 439–450.

Provost, C., Sennéchael, N., Miguet, J., Itkin, P., Rösel, A., Koenig, Z., et al. (2017). Observations of flooding and snow-ice formation in a thinner Arctic sea ice regime during the N-ICE2015 campaign: Influence of basal ice melt and storms. *Journal of Geophysical Research: Oceans*, *122*, 7115–7134. https://doi.org/10.1002/2016JC012011

Pyle, K., Hendry, K., Sherrell, R., Meredith, M., Venables, H., Lagerström, M., et al. (2017). Coastal barium cycling at the West Antarctic Peninsula. *Deep Sea Research Part II: Topical Studies in Oceanography*, *139*, 120–131.

Reigstad, M., Wassmann, P., Riser, C. W., Øygarden, S., & Rey, F. (2002). Variations in hydrography, nutrients and chlorophyll a in the marginal ice-zone and the central Barents Sea. *Journal of Marine Systems*, *38*, 9–29.

Rippeth, T. P., Lincoln, B. J., Lenn, Y.-D., Green, J. M., Sundfjord, A., & Bacon, S. (2015). Tide-mediated warming of Arctic halocline by Atlantic heat fluxes over rough topography. *Nature Geoscience*, *8*, 191–194.

Sirevaag, A., & Fer, I. (2009). Early spring oceanic heat fluxes and mixing observed from drift stations North of Svalbard*. *Journal of Physical Oceanography*, *39*, 3049–3069.

Smedsrud, L. H. (2005). Warming of the deep water in the Weddell Sea along the Greenwich meridian: 1977–2001. *Deep Sea Research I: Oceanographic Research Papers*, *52*, 241–258.

Stroobants, N., Dehairs, F., Goeyens, L., Vanderheijden, N., & Van Grieken, R. (1991). Barite formation in the Southern Ocean water column. *Marine Chemistry*, *35*, 411–421.

Taylor, J. R., Falkner, K. K., Schauer, U., & Meredith, M. (2003). Quantitative considerations of dissolved barium as a tracer in the Arctic Ocean. *Journal of Geophysical Research*, *108*(C12), 3374. https://doi.org/10.1029/2002JC001635

Thomas, H., Shadwick, E., Dehairs, F., Lansard, B., Mucci, A., Navez, J., et al. (2011). Barium and carbon fluxes in the Canadian Arctic Archipelago. *Journal of Geophysical Research: Oceans*, *116*, C00G08. https://doi.org/10.1029/2011JC007120

Weeks, W. F. & Ackley, (1982). *The growth, structure and properties of sea ice* (130 p.). Hanover, NH: U.S. Army Corps of Engineers, Cold Regions Research & Engineering Laboratory.